Self-assembling fluorescent hydrogel for highly efficient water purification and photothermal conversion

Meng Li[a,*], Mengqing Yang[a], Bowen Liu[a], Hongmin Guo[a], Haotian Wang[a], Xiaoning Li[a], Lidong Wang[a], Tony D. James[b,c,*]

[a] *Hebei Key Lab of Power Plant Flue Gas Multi-Pollutants Control, Department of Environmental Science and Engineering, North China Electric Power University, Baoding, 071003, PR China*

[b] *Department of Chemistry, University of Bath, Bath, BA2 7AY, UK*

[c] *School of Chemistry and Chemical Engineering, Henan Normal University, Xinxiang 453007, China.*

Corresponding Author

*Meng Li, E-email: mlincepu@hotmail.com

*Tony D. James, E-mail: t.d.james@bath.ac.uk

Abstract

Employing fluorescent hydrogels for hazardous Hg(II) detection and removal is an efficient method for water purification. However, it remains challenging to establish a fluorescent system with low detection limit and high adsorption capacity that can readily be upcycled into a valuable material resource. Herein, we report on a fluorescent hydrogel with 0D sulfydryl-based carbon dots that are self-assembled with a 3D hydrogel network. The cellulose-based hydrogel exhibited good sensitivity for the detection of Hg(II) over a range from 0 to 40 μM with a limit detection of 3.0×10^{-6} M. The adsorption experiments confirmed that the cellulose-based hydrogel exhibits good

Hg(II) extraction capacity of over 662.25 mg g^{-1} at room temperature, and can effectively reduce the Hg concentration to attain acceptable levels that comply with industrial water standards (0.05 mg L^{-1}). Subsequently, we used a facile strategy to convert the exhausted waste adsorbent by in-situ sulfurization into a suitable material for solar steam generation. The as-prepared upcycled aerogel evaporators exhibited excellent evaporation rates of ~1.30 kg m^{-2} h^{-1} under one sun irradiation. These results not only provide a strategy for heavy metal ion recognition and adsorption, but also provide a route to recycle hazardous waste for seawater desalination.

Keywords: sulfydryl-based carbon dots; fluorescent hydrogel; detection and adsorption; solar steam generation

1. Introduction

As heavy metal pollution intensifies, it poses a significant threat to the environment and as such can harm human beings.[1-3] For example, mercury ions (Hg(II)) are hazardous heavy metal ions that are discharged as effluents by many industrial processes including mining, textiles, and leather production *etc.*[4, 5] Over exposure to Hg(II) in drinking water can result in serious damage to human organs such as the kidney, liver and lungs.[6-8] Therefore, sensitive and effective detection and removal of heavy metal ions from wastewater is urgently required. Amongst the various sensing and purification technologies available, fluorescent hydrogels have drawn much attention due to the low cost, ease of operation and high efficiency.

Among various fluorescent sensing materials, fluorescent carbon dots (CDs) have

emerged as nano sensors for applications in heavy metal ion detection owing to the excellent water solubility, non-toxicity, photostability and easy functionalization.[9-12] Thus, CDs with a high sensitivity and selectivity toward Hg(II) ions can be used as a sensing moiety during the preparation of fluorescent hydrogels. In addition, the zero-dimensional structure of nano CDs helps their self-assembly within the three-dimensional network of the hydrogel, which can increase the number of chelating sites and facilitate capture of Hg(II) ions, thus promoting the sensitivity and adsorption capacities of the material. Cellulose based hydrogels have been widely used for water purification via adsorption due to the high adsorption ability, 3D porous structure and abundance of modifiable and potentially ligating functional groups. For example, carboxymethyl cellulose (CMC) provides not only the skeleton of the hydrogel resulting in a 3D porous structure but also provide many chelating sites for heavy metal ion binding. To the best of our knowledge, there are only a few literature examples of fluorescent hydrogels for both the recognition and adsorption of Hg(II) ions. Therefore, carboxymethyl cellulose hydrogel (CMH) could be used as a scaffold and CDs used as fluorescence based units for the preparation of a fluorescent hydrogel capable of the detection and removal of Hg(II) ions with low detection limit and high adsorption capacities.

The above fluorescent hydrogels could be extensively used for the treatment of heavy metal polluted water. However, the increasing demand for water treatment has led to a rapid generation of abundant end-of-life absorbents owing to their limited life cycle.[13]

Most of the polymeric adsorbents eventually end up in landfills, which is wasteful, unsustainable, and costly. Therefore, to minimize the undesired environmental impact and promote sustainable development, a facile way to upcycle the exhausted materials into valuable products instead of just contributing to already overwhelmed landfills is urgently needed.[14] As such, this problem has motivated the development of methods to ensure the reuse of such hazardous materials to produce freshwater. One approach taken to reuse the materials is the use of solar-to-thermal technology.[15-18] Solar energy has been extensively explored due to its abundant, renewable, and environmentally-friendly properties.[19, 20] Based on the 3D porous structure of the hydrogel, the mercury saturated adsorbents can be sulfurized in situ and used as part of photothermal materials. The 3D hydrogel nanostructure improves the efficiency of photothermal and solar energy conversion by reducing the heat loss caused by the localization of heat at the air-water interface during the heat transfer process.[21, 22] Thus, these materials can then be exploited to absorb solar radiation and generate heat for water desalination. Such usage models provide significant advantages for both the fundamental aspects involved in the reuse of hazardous waste and practical applications for solar-driven water purification and power generation technologies.

Herein, we report an approach to introduce sulfydryl-based carbon dots (CDs-SH) onto a functionalized cellulosed-based hydrogel through hydrogen bonding for the detection and removal of Hg(II) ions from wastewater (Scheme 1). The prepared CDs-SH exhibited excellent sensitivity and selectivity for Hg(II) due to the specific

coordination between Hg(II) and -SH.[23, 24] The CDs-SH were then used as the fluorescent part of the hydrogel sensor to rapidly detect and remove Hg(II) and the mechanism of the quenching phenomenon and adsorption ability was investigated. Furthermore, the exhausted materials were vulcanized and then used for solar steam generation to generate freshwater. This strategy presents great opportunities for preparing multifunctional materials to purify heavy metal ions as well as to upcycle hazardous waste into value-added resources.

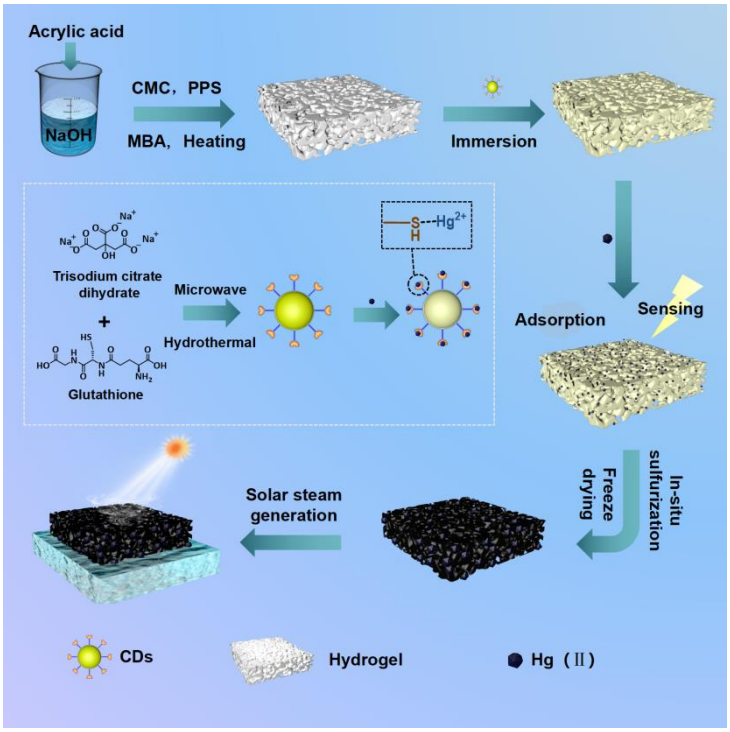

Scheme 1. Schematic illustration of the preparation of CMH-CDs-SH and the detection and removal of Hg(II) ions.

2. Methods

2.1 Materials

The chemicals used are as follows: Sodium citrate (Sinopharm Chemical Reagent Co. Ltd.), Glutathione (Reduced) (Sinopharm Chemical Reagent Co. Ltd.), Sodium carboxymethyl cellulose (CMC) (Aladdin Co., Ltd), Mercuric acetate (Tianjin Komiou

Chemical Reagent, GP), Cadmium Nitrate Tetrahydrate (Sigma-Aldrich Company), Copper sulfate anhydrous (Shanghai Maclean Biochemical Technology Co., Ltd.), Sodium Sulfide (Aladdin Co., Ltd), Lead nitrate (Aladdin Co., Ltd), Chromium nitrate (Aladdin Co., Ltd), Ferric nitrate (Sigma-Aldrich Company), Aluminum Nitrate (Aladdin Co., Ltd), NaOH (Tianjin Komiou Chemical Reagent, GP), Acrylic acid (AA) (Aladdin Co., Ltd), N-methylenebisacrylamide (MBA) (Aladdin Co., Ltd), Potassium persulfate (PPS) (Aladdin Co., Ltd), Sodium chloride (Tianjin HengXing Chemical Reagent co., LTD), Magnesium chloride (Shanghai Yien Chemical Technology Co., Ltd.), Magnesium sulfate (Beijing Chemical Reagent Company), Calcium sulfate dihydrate (Tianjin Komiou Chemical Reagent, GP), Potassium sulfate (Tianjin Damao Chemical Reagent Factory), Calcium carbonate, (Tianjin Fuchen Chemical Reagent Co., Ltd.). DI water was used in all experiments. All of chemicals were used without further purification.

2.2 Instruments

Fluorescence spectra were measured using a F97Pro fluorescence spectrophotometer. AFS 933 atomic fluorescence spectrometer was used for measuring the concentration of Hg(II) ions. The Cu(II) ions and Cd(II) ions were determined using a AA-6800 flame atomic absorption spectrometer. The UV–Vis is absorption spectra for the samples were collected using a T6 New Century ultraviolet–visible spectrophotometer.

2.3 Fabrication of carbon dots (CDs-SH)

CDs are prepared by hydrothermal and microwave reaction. Sodium citrate (1 g) and glutathione (0.1 g) were added to DI water (30 mL) with stirring, and sonication for 30 min to produce a homogeneous solution. Finally, the solution was transferred into a Teflon-lined stainless-steel autoclave (100 mL) and heated at 200 ℃ for 4 h. The autoclave was then cooled to 20 °C and the mixture was heated using a 600 W domestic microwave oven for 4 min. The resultant mixture was then filtered using a 0.1 mm filter to remove large particles resulting in a purified CD solution. Finally, the purified yellow solution was dried using a freeze dryer to obtain CD powder.

2.4 Preparation of fluorescent hydrogels

CMH-CDs-SH: MBA (0.04 g) and CMC (0.263 g) were dissolved in AA (3.8 mL) and 1.0 wt% NaOH solution (11.0 mL), and then sonicated for 1 h. Subsequently, PPS (0.2 g) was added, and the solution was incubated in a water bath at 65 ℃ for 2 h to obtain CMH hydrogel. Finally, the synthetic cellulose hydrogel was immersed in CDs-SH solution (1 g/L). After 24 h, it was washed 3 times with DI water to obtain fluorescent hydrogel CMH-CDs-SH. The fluorescent hydrogel CMH-CDs-SH was then freeze-dried for the adsorption experiments.

Acrylic acid hydrogel (AAH): MBA (0.04 g) and AA (3.8 mL) were dissolved in 1.0 wt% NaOH solution (11.0 mL). Then, PPS was added to the solution after sonication for 1 h. Finally, the mixed solution was stirred at 65 ℃ for 2 h to obtain the AAH.

2.5 Characterization

Scanning electron microscopy (HitachiS-4800 SEM) and transmission electron

142 microscopy (JEM-2100) were used to investigate the morphology and nanostructure of
143 the as prepared cellulose hydrogel. JEM 2100F transmission electron microscope was
144 employed to determine the transmission electron microscopic (TEM) images. Fourier
145 transform infrared (FT-IR) spectra were obtained on Thermo Electron Nicolet iZ10 over
146 a range of 4500-400 cm^{-1}. The morphology of the samples was determined using a
147 scanning electron microscopy (SEM, Hitachi-s4800). The surface elemental
148 composition of the aerogel was characterized using a Thermo Scientific Ultra Dry SDD
149 Energy-dispersive X-ray spectroscope (EDS). The elemental compositions for the
150 samples were measured by X-ray photoelectron spectroscopy (XPS) using a
151 ESCALAB250Xi spectrometer.

152 **2.6 Fluorescence detection**

153 A F97Pro fluorescence spectrophotometer was used for measurement. 25 μg/mL of
154 CDs-SH was prepared in water. A series of metal ions including Hg(II), Cu(II), Cr(III),
155 Fe(III), Al(III), Ni(II), Pb(II), and Cd(II) were placed into the CDs-SH solution for
156 selective analysis. For the fluorescence spectra of the cellulose gel, a gel slice with
157 deionized water (2 mL) was placed into the quartz cuvette. Then 0-40 μM of Hg(II)
158 solution was added and the fluorescence behavior was then monitored.

159 **2.7 Adsorption detection**

160 Batch adsorption experiments were used to explore the adsorption properties of Hg(II)
161 with the fluorescent hydrogel. The adsorption process was performed by adding 10 mg
162 of the freeze-dried hydrogel into 10 mL of mercury solution (100 mg mL^{-1}) with

shaking for 2 h at 293 K in a thermostatic shaker bath.[25] All Hg(II) ion solutions in the article are prepared by dissolving mercury acetate in DI water. The Hg(II) concentration was measured by a AFS 933 atomic fluorescence spectrometer. The adsorption efficiency (η) and equilibrium adsorption capacity (Q_e) were determined using equations (1) and (2):

$$Q_e = \frac{(C_0 - C_e)}{m} V \quad (1)$$

$$\eta = \frac{C_0 - C_e}{C_0} \times 100\% \quad (2)$$

Where C_0 is the initial concentration of the Hg(II) solution (mg L^{-1}), C_e is the equilibrium concentration of the Hg(II) solution (mg L^{-1}), V and m are the volume of the solution (L) and the weight of the freeze-dried CMH-CDs-SH (g), respectively.

2.8 Adsorption kinetics

To study the adsorption mechanism, the pseudo-first-order (Eq. 3) and pseudo-second-order models (Eq. 4)[26] were used to analyze and describe the experimental data, the equations of which are expressed as follows:

$$\ln(Q_e - Q_t) = \ln Q_e - k_1 t \quad (3)$$

$$\frac{t}{Q_t} = \frac{1}{k_2 Q_e^2} + \frac{t}{Q_e} \quad (4)$$

In which Q_e and Q_t (mg g^{-1}) are the adsorbed amounts of Hg(II) on the cellulose gel at equilibrium and time (min); and k_1 (min^{-1}) and k_2 (g (mg min)$^{-1}$) represent the rate constant of pseudo-first-order and pseudo-second-order models, respectively.

2.9 Adsorption isotherm

The adsorption isotherms were used to investigate the adsorption performance

between Hg(II) and CMH-CDs-SH.[27, 28] The formulas of the Langmuir (Eq. 5) and Freundlich models (Eq. 6) are described as follows:

$$Q_e = \frac{Q_m K_L C_e}{1+K_L C_e} \quad (5)$$

$$\ln Q_e = \frac{1}{n}\ln C_e + \ln K_F \quad (6)$$

In which Q_e and Q_m (mg g^{-1}) represent the adsorbed amount of Hg(II) on the cellulose gel at equilibrium and the maximum adsorption capacity; C_e (mg L^{-1}) represents the equilibrium concentration of Hg(II); K_L and K_F are the Langmuir and Freundlich constants, respectively; n is the Freundlich empirical parameter.

2.10 Adsorption thermodynamics

To further investigate the thermodynamic properties between the Hg(II) and CMD-CDs-SH, adsorption experiments were carried out at 293, 313 and 333 K. The thermodynamic values of △G, △H and △S for the adsorption of Hg(II) on the adsorbents were calculated according to the van't Hoff equation:

$$K_c = \frac{1000 C_a}{C_e} \quad (7)$$

$$\Delta G = -RT\ln K_c \quad (8)$$

$$\ln K_c = \frac{\Delta S}{R} - \frac{\Delta H}{RT} \quad (9)$$

$$\Delta G = \Delta H - T\Delta S \quad (10)$$

In which K_c (mL g^{-1}) is the partition coefficient; C_a (mg g^{-1}) and C_e (mg L^{-1}) represent the adsorbed amount of Hg(II) on the cellulose gel and the equilibrium concentration of Hg(II), respectively; T is the temperature; R is the gas constant (8.314 J mol^{-1} K^{-1}); △G (kJ mol^{-1}), △H (kJ mol^{-1}) and △S (J K^{-1} mol^{-1}) are the Gibbs free energy changes,

enthalpy change and entropy change, respectively.

2.11 Competitive adsorption experiments in a binary system

10 mg of CMH-CDs-SH was placed in a plastic centrifuge tube, including a mixed solution of two metal ions (10 mL), a mixed solution of Hg(II)/Cu(II) and Hg(II)/Cd(II) in the range of 10-1000 mg L^{-1}. The plastic centrifuge tube was then shaken for 3 h at 293 K and the metal ion solution was collected for subsequent tests. There are three types of effects in the multi-component system: synergy ($Q_{mix}/Q_0>1$), antagonism ($Q_{mix}/Q_0<1$) and non-interaction ($Q_{mix}/Q_0=1$).[29] The interaction between the two components in the binary mixture can be derived from the ratio of the Q_0 of a single component to the Q_{mix} of the single component in the binary component.

A competitive Langmuir model [Eq. (11)] [30-32] was used to analyze the data obtained in the binary system. Eq. (11) can also be rearranged into the following equation Eq. (12) and then arranged into a binary system. The equilibrium adsorption data were validated using the Marquardt percentage standard deviation (MPSD) according to the following Eq. (13).

$$Q_{e,i} = \frac{Q_{max,i} K_{L,i} (C_{e,i})}{1+\sum_{j=1}^{N} K_{L,j} (C_{e,j})} \quad (11)$$

$$Q_{e,1} = \frac{Q_{max,1} K_{L,1} (C_{e,1})}{1+K_{L,1} C_{e,1}+K_{L,2} C_{e,2}} \quad (12)$$

$$MPSD = 100 \times \sqrt{\frac{1}{N-P} \sum \left(\frac{Q_{i,e}^{exp} - Q_{i,e}^{cal}}{Q_{i,e}^{exp}} \right)^2} \quad (13)$$

Where, $C_{e,i}$ is the equilibrium concentration of the i-th metal ion (mg L^{-1}), and $K_{L,i}$ is the adsorption constant (L mg^{-1}). $Q_{i,e}^{cal}$ is the experimental adsorption capacity (mg g^{-1}), $Q_{i,e}^{exp}$ is the theoretical adsorption capacity (mg g^{-1}), N is the total number of

226 experiments and P is the number of parameters in the model.

227 **2.12 Competitive adsorption experiments in ternary systems**

228 10 mg of CMH-CDs-SH was placed in to a 10 mL mixed solution containing Hg(II),
229 Cu(II) and Cd(II)ions with a varying range of 10-200 mg L^{-1}, respectively. The mixture
230 was shaken for 120 min at 293 K and collected for the subsequent testing.

231 **2.13 Recyclability**

232 20 mg of CMH-CDs-SH was added to 20 mL of Hg(II) solution (100 mg L^{-1}) at 293
233 K for 120 min. Then the Hg(II)-loaded hydrogel was regenerated by immersing the
234 adsorbent in 20 mL of HCl solution (1.0 mol L^{-1}) and shaking at room temperature for
235 720 min. The regenerated hydrogel was used in another cycle after washing with DI
236 water until a neutral pH was achieved

237 **2.14 Fabrication of S-loaded aerogel**

238 Initially, CMH-CDs-SH was used to adsorb Hg(II) (1000 mg L^{-1}) ions for 12 h at
239 room temperature. After being taken out from the solution, the Hg(II) ion-loaded gel
240 was washed with deionized water to remove any non-absorbed Hg(II) ions. Then, the
241 remaining adsorbent was immersed in Na_2S solution for 12 h. Based the adsorption
242 capacity of Hg(II) by CMH-CDs-SH, the molar ratios of mercury ions absorbed on the
243 adsorbents to sulfur were 1:1; 1:2; 2:1. Finally, the gel was treated with distilled water
244 to reach a neutral pH, and then dried in a freeze-drying oven to obtain the S-loaded
245 aerogel.

246 **2.15 Solar steam generation**

The water evaporation experiments of CMH-HgS_x were performed in a crystallizing dish (100 mL) with 70 mL of distilled water and then irradiated under a solar simulator with 100 mW cm^{-2} at room temperature and a humidity of about 50%. During the experiment, the mass changes of the system was measured on an electronic balance. Temperature changes were monitored in real time by an infrared camera. The energy efficiency (η) can be obtained according to Eq. (14) below.[33]

$$\eta = \frac{mh_V}{C_{opt}q_i} \quad (14)$$

Where m is the mass flux under steady-state conditions; h_V is the enthalpy of evaporation of water in the sample (2444 J g^{-1}). C_{opt} represents the optical concentration and q_i represents the solar irradiation power on the adsorber surface (100 mW cm^{-2}).

3. Results and discussion

3.1 Characterization of CDs-SH and CMH-CDs-SH

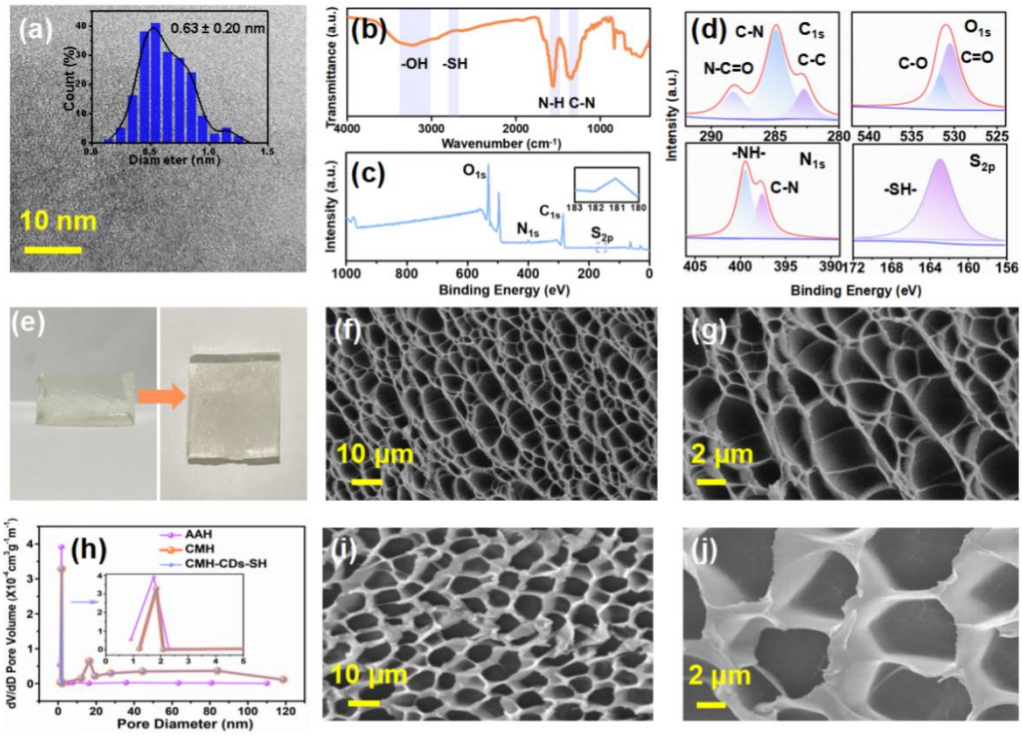

Fig. 1. Characterization of CDs-SH and CMH-CDs-SH. (a) TEM image of CDs-SH (Insert: Particle size distribution of the CDs-SH); (b) FTIR spectra of CDs-SH; (c, d) XPS survey spectrum of wide scan, C_{1s}, O_{1s}, N_{1s}, and S_{2p} for CDs-SH; (e) The images of CMH-CDs-SH; SEM images of (f) AAH and (i) CMH-CDs-SH, high magnification SEM images of (g) AAH and (j) CMH-CDs-SH; (h) Particle size distribution of AAH, CMH and CMH-CDs-SH.

Sulfydryl-rich fluorescent carbon dots (CDs-SH) were prepared by hydrothermal and microwave reaction. From the TEM image (Fig. 1a) the CDs-SH are evenly dispersed with an average diameter of 0.63 ± 0.2 nm. FT-IR spectroscopy was then used to characterize the functional group of the CDs-SH (Fig. 1b). The broad band at 3430 cm^{-1} is associated with O-H stretching vibrations and the peak at 2610 cm^{-1} is attributed to S-H stretching vibrations.[34, 35] Meanwhile, the peaks at around 1390 cm^{-1} and 1570 cm^{-1} are in accordance with the vibrations of C-N and N-H, respectively. The full XPS spectrum of CDs-SH confirmed that the C, O, N and S elements are present in the CDs-SH and the peaks at 530.0, 401.1, 285.1 and 163.9 eV were ascribed to the O_{1s}, N_{1s}, C_{1s} and S_{2p}, respectively (Fig 1c). The C_{1s}, O_{1s} N_{1s} and S_{2p} high resolution XPS spectra are given in Fig. 1d. In the C_{1s}, three peaks at 282.8, 285.0 and 288.2 eV are ascribed to the C-C, C-N and N-C=O. There were two peaks in the N_{1s} spectrum at 397.1 eV and 399.5 eV, which could be attributed to the C-N and N-H. While the O_{1s}, the peaks at 530.4 and 531.7 eV could be attributed to the C=O and C-O respectively. For the S_{2p}, the peak at161.2eV could be attributed to S-H, the XPS results further confirmed that the existence of -SH on the CDs-SH.[36, 37] Subsequently, the fluorescent hydrogel was prepared via immersing cellulose-based hydrogel (CMH) with CDs-SH facilitated by hydrogen bond driven assembly (Fig. 1e). CMH provides a natural skeleton and results

in a 3D porous network structure to provide a channel for the transmission of heavy metal ions. Then it is soaked with CDs-SH solution to generate a fluorescent hydrogel (CMH-CDs-SH). CDs-SH can be not only used as a fluorescent sensor, but also provides binding sites for Hg(II) ions. The sulfhydryl groups on the surface of the CDs can provide a large quantity of available binding sites for chelation with Hg(II).[38, 39] As shown in Fig. S1, it can be seen from the EDS diagram that homogeneous C, O, N and S elements exist in the CMH-CDs-SH, which also indicated that the CDs-SH are uniformly dispersed throughout the hydrogel. SEM was used to determine the morphology of the acrylic acid hydrogel (AAH) (Fig. 1f, g) and CMH-CDs-SH (Fig. 1i, j). Both AAH and CMH-CDs-SH exhibit a 3D porous network structure. These 3D network structures can increase ion migration speeds and enhance adsorption capacity.[25] The pore size distribution desorption-desorption isotherms (Barrett−Joyner−Halenda) indicated that the average pore size of the CMH with or without CD loading was nearly the same (Fig. 1h). This result confirmed that CDs did not change the pore size of the CMH. Compared with AAH, CMH-CDs-SH exhibited a higher surface area (4.59 $m^2 g^{-1}$), pore volume (0.0274 $cm^3 g^{-1}$) and average pore size (23.85 nm). Meanwhile, CMH-CDs-SH displayed an abundant mesoporous structure with pore diameter of 18 nm, which could promote adsorption of metal ions due to abundance of active sites dispersed throughout the CMH-CDs-SH, thus improving the adsorption ability. [40, 41] The XRD pattern of CDs-SH (Fig. S2) shows that the peak value is at about 31°, indicating that the prepared CDs are mainly amorphous carbon

atoms which is similar to graphene carbon nanomaterials. Through comparison between CMH and CMH-CDs-SH, it was found that CMH CDs-SH has an XRD peak at 31°, indicating that the CMH was successfully functionalized with CDs-SH.

3.2 Fluorescence properties of CDs-SH and CMH-CDs-SH

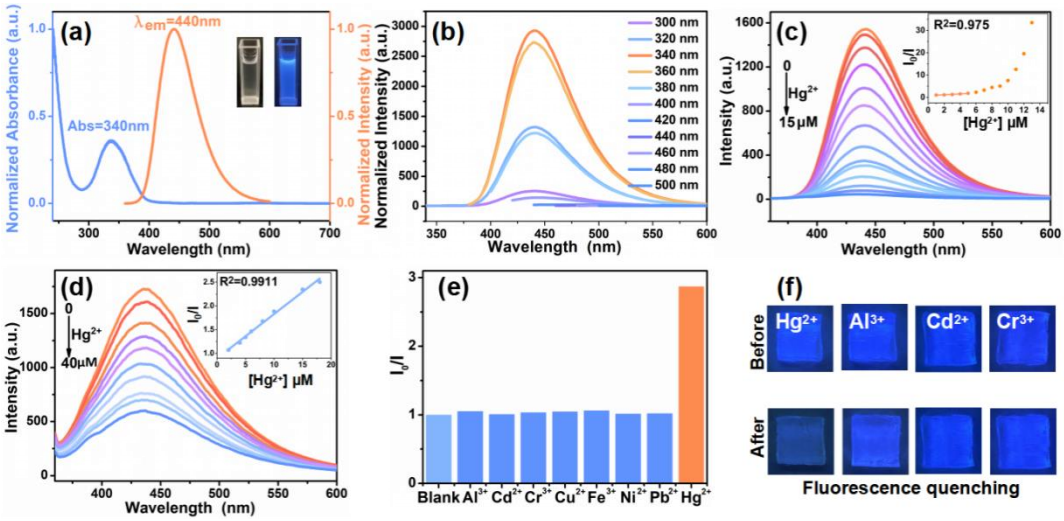

Fig. 2. Fluorescence properties of CDs-SH and CMH-CDs-SH. (a) Normalized absorbance and fluorescence emission spectra of CDs-SH in aqueous solution (25 μg mL^{-1}); (b) FL spectra of CDs-SH (25 μg mL^{-1}) aqueous solutions at different excitation wavelengths; (c) Fluorescence emission spectra of the CDs-SH upon addition of various concentrations of Hg(II) (0-15 μM) (λ_{ex}= 340 nm) (Insert: The relationship between fluorescence intensity (I_0/I) and Hg(II) from 0 to 15 μM); (d) Fluorescence emission spectra of CMH-CDs-SH in aqueous solution upon addition of various concentrations of Hg(II) (0-40 μM) (λ_{ex}= 340 nm) (Insert: The relationship between fluorescence intensity (I_0/I) and Hg(II) from 0 to 40 μM); (e) Fluorescence ratio of fluorescent hydrogel CMH-CDs-SH added with various metal ions (100μM); (f) Fluorescence quenching for synthesized CMH-CDs-SH after metal adsorption.

To explore the fluorescence properties of the CDs-SH and CMH-CDs-SH, UV–vis absorption and emission spectra of the CDs in aqueous solution were investigated (Fig. 2a). The prepared CDs-SH displays a UV-visible absorption band at 340 nm and a fluorescence emission peak at 450 nm. In addition, it was found that the CDs-SH exhibited blue fluorescence under a UV lamp.[42, 43] Additionally, a solution of CDs-SH exhibited the most intense intensity at around 440 nm with excitation at 340 nm

(Fig. 2b). In order to understand the Hg(II) recognition behavior, the fluorescence spectrum of CDs-SH upon the addition of Hg(II) was investigated. In the presence of Hg(II) ions, the fluorescence intensity of CDs-SH was significantly quenched (Fig. 2c). This quenching effect can be attributed to the affinity between Hg(II) and the functional groups, such as sulfhydryl groups on the surface of CDs-SH.[44] CDs-SH exhibited a linear relationship between the I_0/I and the concentration of Hg(II) (0~15 μM), with a correlation coefficient of 0.975. Based on the Stern-Volmer formula, the quenching constant KSV was found to be 0.008. The limit detection for the CDs-SH for Hg(II) was determined to be 2.7×10^{-7} mol L^{-1} according to the 3δ/k (where δ represents the standard deviation of the blank CDs-SH solution, and k represents the slope of the linear plot.). Furthermore, the selectivity of the CDs-SH was evaluated by the addition of different metal ions, and only Hg(II) exhibited a significant fluorescence decrease, while the other metal ions had little effect on the fluorescence of the CDs-SH. In contrast, in the presence of Hg(II) ions, the intensity ratio (I_0/I) increased by 691.90%, indicating that CDs-SH has excellent selectivity for Hg(II) (Fig. S3). Meanwhile, inspired by the above fluorescence performance, the fluorescent hydrogel containing CDs-SH (CMH-CDs-SH) was prepared for the recognition and removal of Hg(II) ions. As shown in Fig. S4, it can be seen that the CMH exhibits no fluorescence change with an increasing concentrations of Hg(II) ions. While, the emission intensity of the CMH-CDs-SH at about 440 nm decreases after addition of Hg(II) ions, indicating that the CDs-SH plays an important role in Hg(II) sensing (Fig. 2d).[45] When the Hg(II) ions

were adsorbed and trapped in the fluorescent hydrogel, the inner filter effect resulted in fluorescence quenching. The fluorescence intensity ratio (I_0/I) is linearly proportional to the Hg(II) concentration over a range of 0-40 μM. The detection limit of the CMH-CDs-SH was 3.0×10^{-6} mol L^{-1}, exhibiting a good sensitivity for the Hg(II). Furthermore, the selective detection of the fluorescent hydrogel CMH-CDs-SH towards different metal ions was evaluated. As shown in Fig. 2e, the selectivity of the fluorescent hydrogel CMH-CDs-SH for Hg (II) is superior to other potentially interfering ions. The fluorescence of Cr(III); Fe(III); Al(III); Cu(II); Cd(II); Ni(II) and Pb(II) ions was hardly affected while Hg(II) exhibited rapid and complete fluorescence, quenching of the CMH-CDs-SH (Fig. 2f, S5), which may be explained by the fact that Hg(II) ions have good electron-capturing ability. Therefore, more electrons are transferred from the CD to Hg(II) ions, resulting in the greatest fluorescence quenching.[45-47] These results confirmed the excellent selectivity of CMH-CDs-SH for Hg(II) ions.

3.3 Adsorption capacities of the CMH

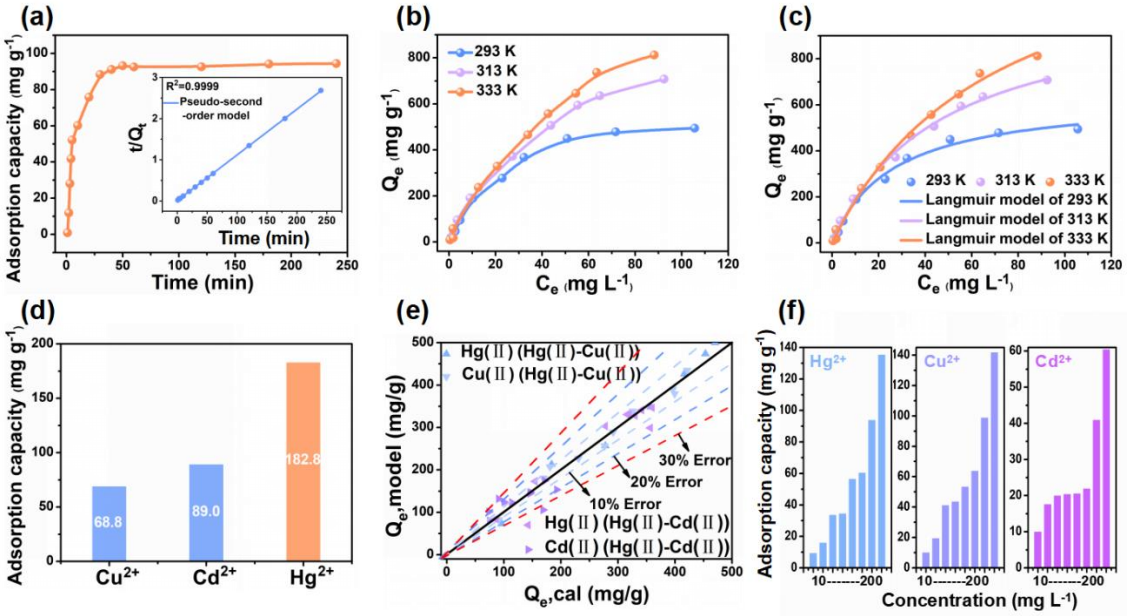

Fig. 3. Adsorption capacities of the CMH-CDs-SH. (a) The effect of different contact time on uptake ability for Hg(II) (Insert: Fitting results of pseudo-second-order model); (b) The adsorption capacity of CMH-CDs-SH with different initial concentrations at different temperatures; (c) Fitting results of Langmuir isotherms model for Hg(II); (d) The adsorption capacity of CMH-CDs-SH in a single solution; (e) The adsorption capacity of the experimental and calculated values of CMH-CDs-SH in a binary solution mixture (20°C, pH=3.5 and 120 min); (f) The adsorption capacity of CMH-CDs-SH in a ternary solution mixture.

Furthermore, we also evaluated the adsorption capacity of CMH-CDs-SH for Hg(II) to obtain the best conditions for removing Hg(II). First, the effect of pH on the adsorption capacity of CMH-CDs-SH was evaluated over a pH range from 1.0 to 6.0. As shown in Fig. S6, as the pH value increases, the adsorption capacity also increases, and reaches a maximum at pH 5.0. Therefore, the optimal pH conditions are around 5.0. To understand the adsorption mechanism, the influence of contact time and adsorption capacity was determined. The adsorption of Hg(II) by CMH-CDs-SH is rapid at first, then slows down, and finally reaches equilibrium after 1h. These results are used to fit the pseudo-first-order kinetic model and the pseudo-second-order kinetic model. The linear fitting results and kinetic parameters are shown in Table S1, Fig. 3a insert and

Fig. S7. Clearly, the adsorption of Hg(II) by CMH-CDs-SH fits a pseudo-second-order model (R^2= 0.999). These results indicated that the adsorption mechanism of Hg(II) is mainly chemical adsorption.

To further estimate the adsorption properties, the effect of temperature on the adsorption of CMH-CDs-SH was examined. As shown in Fig. 3b, with an increase of temperature, the adsorption capacity exhibited an obvious increasing trend (The maximum adsorption capacity increased from 662.25 mg g^{-1} to 1346.83 mg g^{-1}), indicating that an increase of temperature is conducive to the adsorption of Hg(II). Meanwhile, this result can be also confirmed by the calculated thermodynamic parameters (Table S2), the △H is positive indicating that CMH-CDs-SH adsorption of Hg(II) is an endothermic process, while △S is negative, indicating that adsorption of Hg(II) is a spontaneous process. In addition, with an increase of temperature, the decrease of △G value indicated that a higher temperature is conducive to the adsorption of Hg(II), which is consistent with the experimental results.

To evaluate the isotherm model. The dependence of CMH-CDs-SH on the concentration of a wide range of initial mercury ion concentrations was evaluated. The adsorption capacity of the CMH-CDs-SH increased with an increase of the initial Hg(II) concentration. In addition, compared to the cellulose-based hydrogel (CMH) at 293 K, the CMH-CDs-SH exhibited a slightly higher adsorption capacity, suggesting that the CDs promote the extraction efficiency of Hg(II) (Fig. S8). The fitting results of Langmuir and Freundlich adsorption isotherms for the CMH-CDs-SHs are shown in

Fig. 3c and S9, respectively. The parameters in Table S3 indicate that the R^2 value of the Langmuir model is higher than that of the Freundlich model at 293~333 K. The fitting results indicate the adsorption of Hg(II) with monolayer coverage. According to the fitting parameters of the Langmuir model, the maximum adsorption capacity of the CMH-CDs-SH for Hg(II) at 293 K is 662.25 $mg \cdot g^{-1}$.

Similarly, the recyclability of the adsorbents is of great importance for environmental applications. To reveal the recyclability of the CMH-CDs-SH, CMH-CDs-SH regeneration was achieved by immersing the adsorbent in hydrochloric acid solution for 2 h. Fig. S10 shows that after four cycles of desorption, the adsorption efficiency of the CMH-CDs-SH for Hg(II) ranges from 98.8% to 88.3%, which indicates that the Hg(II) ion uptake ability of the CMH-CDs-SHs only slightly decreases in repeated adsorption-desorption cycles. Therefore, CMH-CDs-SH exhibits good recyclable properties and can be used for practical applications.

Generally, industrial wastewater contains a variety of heavy metal ions at different concentrations.[48-51] Therefore, the development of multi-component adsorption materials is the key for effective water treatment technology.[52] In addition to the adsorption of Hg(II), CMH-CDs-SH was used to adsorb Cu(II) and Cd(II) ions. As shown in Fig. 3d, in a single system, the material exhibits good adsorption performance for Cu(II), Cd(II) and Hg(II), with adsorption capacities of 68.8, 89.0 and 182.8 $mg \cdot g^{-1}$, respectively. For the binary system, a two-component adsorption system consisting of Hg(II)-Cu(II) and Hg(II)-Cd(II) were evaluated, and the results were fitted using a

Langmuir competition model. To further check the accuracy of the model, a comparison between the theoretical prediction and the experimental values are given in Fig. 3e. The MPSD values of the isotherm model range from 8 to 30 (Table S4). The results indicate that the Langmuir competition model is suitable for the binary system. From the calculated Q_{mix}/Q_0 value range from 0.381 to 0.831, it can be concluded that there is an antagonistic effect in the binary adsorption process. For the ternary system (Fig. 3f), with increase of the initial concentration, the adsorption capacity of the three ions shows an increasing trend. Compared with the single component system, CMH-CDs-SH has a lower adsorption capacity for these metal ions. These phenomena may be attributed to the occurrence of antagonism effects on the adsorbents.

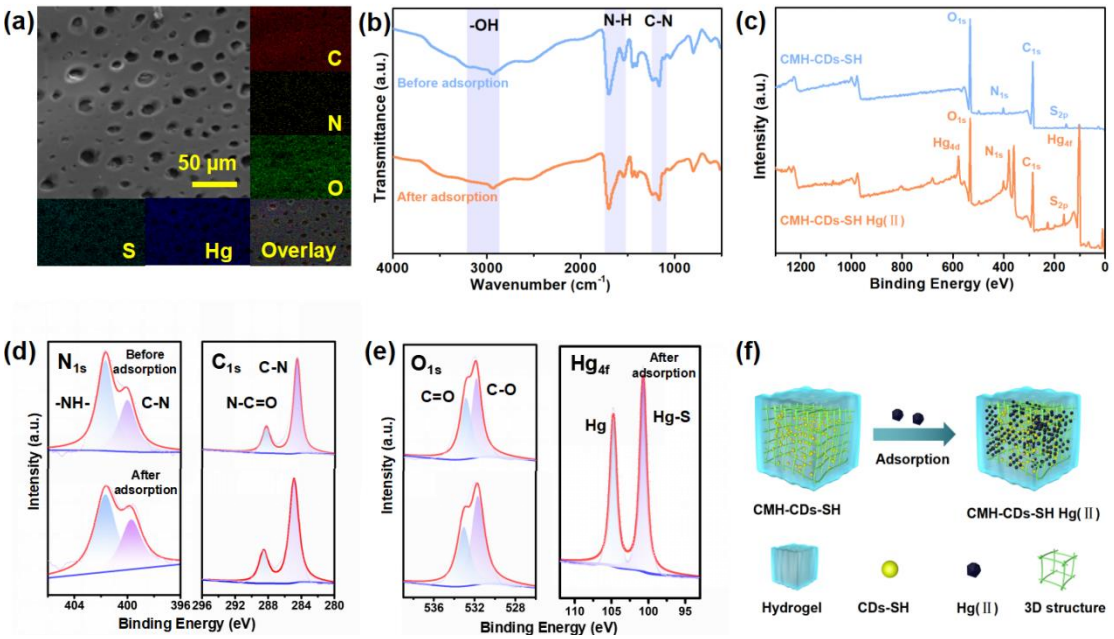

Fig. 4. Characterization of CMH-CDs-SH. (a) SEM and mapping images of CMH-CDs-SH/Hg(II); (b) FTIR spectra of CMH-CDs-SH before and after adsorption; (c-e) XPS survey spectrum of wide scan, C_{1s}, O_{1s}, N_{1s}, and Hg_{4f} for CMH-CDs-SH and CMH-CDs-SH/Hg(II); (f) Investigation of the adsorption mechanism of CMH-CDs-SH with Hg(II).

The 3D fluorescent CMH-CDs-SH exhibited good adsorption and sensing ability for

Hg (II). EDS-mapping, FTIR and XPS spectra were further used to determine the adsorption mechanism. As shown in Fig. 4a, the cross-sectional SEM images display porous structures of the CMH-CDs-SH/Hg(II). In addition, it can be seen from the EDS diagram that C, O, N, S and Hg elements were dispersed homogenously in the CMH-CDs-SH with adsorbed Hg(II), which is consistent with the results of the XPS. Before and after adsorption, slight changes in the stretching vibration of the -OH (3307cm^{-1}), -NH (1582cm^{-1}) and C-N (1036cm^{-1}) were attributed to the adsorption of Hg(II) (Fig. 4b). In the high-resolution XPS spectra of CMH-CDs-SH, the C, O and N elements in CMH-CDs-SH are observed (Fig. 4c-e). The N_{1s} displayed two components related to -NH- at 401.1 eV and C-N at 397.8 eV. For O_{1s}, the typical peaks at 533.0 and 530.9 eV are assigned as C=O and C-O, and the O_{1s} at 531.3 eV can be ascribed as a carboxyl group. For the C_{1s}, the typical peaks at 288.0 and 285.2 eV were assigned to N-C=O and C-N, which correspond to the oxygen-containing and nitrogen-containing functional groups in the CMH-CDs-SH (Fig. 4d).

Based on these results, the adsorption and sensing mechanism of the 3D fluorescent hydrogel CMH-CDs-SH for Hg(II) is shown in Fig. 4f. When Hg(II) ion solution enters the CMH-CDs-SH material, the Hg(II) ions undergo specific binding with the thiol group. Moreover, the porous 3D structure provides Hg(II) ion transport channels, and promotes the diffusion of Hg(II) ions from the external surface of the hydrogel to the interior. As such Hg(II) ions are adsorbed by the internal regions of the hydrogel, and bound to the carboxyl and hydroxyl groups of the hydrogel. Therefore, the 3D porous

fluorescent hydrogel exhibits excellent adsorption capacity for Hg(II). When Hg(II) ions are added, Hg(II) ions are adsorbed by the CDs due to the specific binding with the sulfydryl groups, resulting in a rapid fluorescence response for Hg(II) ions.

Moreover, from a comparison of the different materials published for Hg(II) detection and removal in Table S5, CMH-CDs-SH exhibits better detection and removal capabilities. Furthermore, the exhausted materials can be vulcanized and then used for solar steam generation to generate freshwater, which provides a route to recycle hazardous waste for seawater desalination.

3.4 Investigation of solar steam generation efficiency

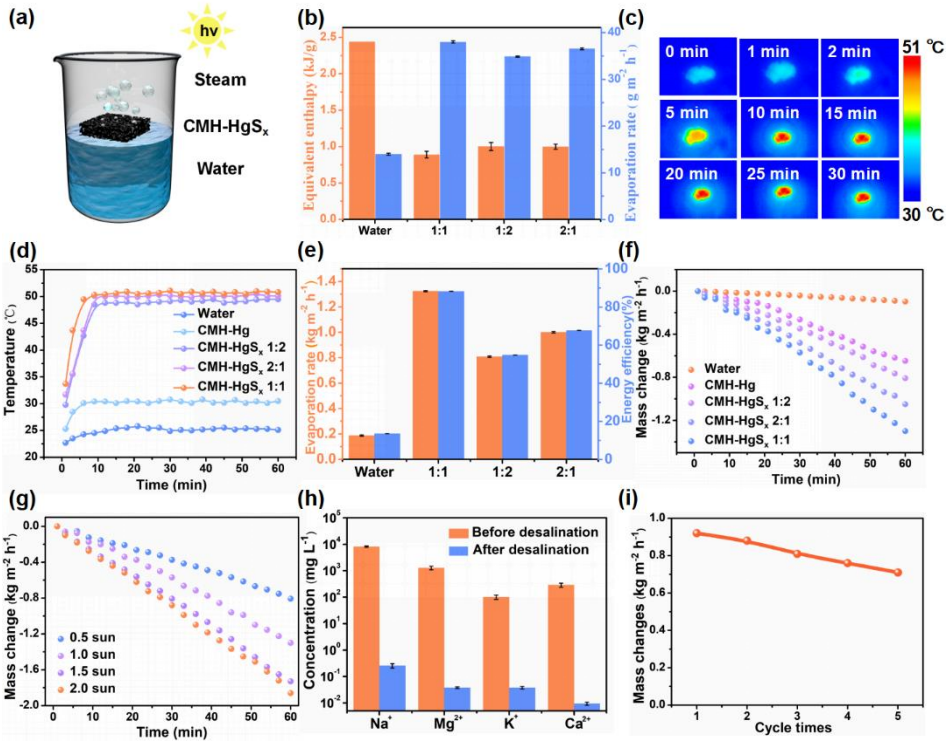

Fig. 5. Performance of solar steam generation. (a) Schematic of solar steam generation using CMH-HgS_x; (b) Water evaporation rate under dark conditions and the calculated equivalent enthalpy for CMH-HgS_x; Infrared photographs (c) and temperature changes (d) under one sun irradiation (100 mW cm^{-2}); (e) Evaporation rate and energy efficiency of CMH-HgS_x with different Hg/S ratios; (f) Time-dependent mass change of the gel under one sun irradiation; (g) Water mass changes as a function of solar irradiation time

for CMH-HgS_x at different optical concentrations; (h) The purification performance of CMH-HgS_x for simulated sea water; (i) Cycling properties of CMH-HgS_x under one sun irradiation.

The limited life cycle of fluorescent hydrogels, and the increasing demand for water treatment has led to the rapid production large amounts of exhausted absorbents as waste. Therefore, to promote sustainable development and to reduce environmental pollution, a facile way to upcycle the exhausted materials into valuable products is urgently required. One approach taken to reuse the materials is the use of solar-to-thermal technology. CMH-CDs-SH not only exhibits good ability to remove various metal ions but provide an opportunity for use in solar steam power generation. First, the CMH-HgS_x is synthesized by the vulcanization reaction between the saturated adsorbent containing Hg(II) ions and Na_2S solution. As shown in Fig. 5a, the color of the CMH changed to black after the sulfurization process. The black CMH-HgS_x can be used as a "solar absorber" to convert light into heat. Therefore, the material can be used to absorb solar radiation and generate heat for seawater desalination.[53] The binding states and quantitative chemical compositions of the CMH-HgS_x samples were determined by XPS analyses. As shown in Fig. S11 and Table S6, the C_{1s} exhibits two components related to N-C=O at 288.7 eV and C-N at 284.8 eV, which correspond to the oxygen-containing and nitrogen-containing functional groups in the CMH-HgS_x. For O_{1s}, typical peaks at 532.7 and 531.3 eV are assigned as C=O and C-O. For N_{1s}, the peaks at 398.9 and 401.2 eV on the CMH-HgS_x are attributed to the C-N and -NH-. It was observed that the CMH-HgS_x contains a large amount of S (8.14%) and Hg (10.39%), while CMH-CDs-SH/Hg(II) reveal much lower levels of S. This result

showed that S was successfully incorporated into the CMH-HgS_x. Meanwhile, double peaks corresponding to HgS were observed at 162.2 eV and 161.3 eV after in-situ vulcanization. These results confirmed that Na_2S substances were used for the formation of HgS on CMH-HgS_x (Fig. S11e).[54] As for the Hg_{4f} peak (Fig. S11f), double peaks at 104.2 and 100.1 eV were designated as Hg-S, suggesting that HgS was the main Hg species within the CMH-HgS_x.[55] Initially, the water evaporation rate of CMH-HgS_x samples with different Hg/S ratios (molar ratios of mercury to sulfur: 1:1, 1:2, 2:1) were carried out under dark conditions to explore the effect on the evaporation rate of water. As shown in Fig. 5b, the evaporation rate under dark conditions was recorded under closed conditions with a temperature of 30 °C, ambient air pressure, and a relative humidity of ≈ 60%. The results indicated that the water evaporation rates of CMH-HgS_x samples with different Hg/S ratios were almost the same, however higher than that of bulk water. Then the corresponding equivalent enthalpy is estimated according to the previously established formula, which indicates that CMH-HgS_x reduce the energy cost of evaporation, and the best molar ratio is under the conditions of 1:1 (mercury to sulfur). The temperature changes of the CMH-HgS_x with different Hg/S ratios were measured using an infrared camera under one sunlight irradiation (Fig. 5c and S12). The surface temperature of the CMH-Hg and CMH-HgS_x (1:1) rapidly increased to 29.4°C and 51.0°C within 30 minutes, and then reached a steady state (Fig. 5d). CMH-HgS_x exhibits a higher performance than CMH-Hg, which may be due to the better optical properties of black CMH-HgS_x when compared with the light yellow

CMH-Hg, CMH-HgS_x accelerates the conversion of light into heat.[56] The result indicated that the CMH-HgS_x has an excellent heat localization effect, which contributes to solar steam generation. Subsequently, the steam-generation efficiency of the CMH-Hg and CMH-HgS_x (1:1, 1:2, 2:1) were calculated by measuring the weight of water evaporation against irradiation time under one sun illumination. From Fig. 5e, f, the water evaporation rate of CMH-HgS_x (1:1) was 1.30 kg m^{-2} h^{-1}, which is a higher performance when compare to 0.67 kg m^{-2} h^{-1} for CMH-Hg. The corresponding energy efficiency of CMH-HgS_x was calculated to be 88.3% under one sun illumination, and as such exhibit's great potential as a solar evaporator. In addition, we evaluated the water evaporation capacity of CMH-HgS_x (1:1) by changing the intensity of incident sunlight (Fig. 5g). The water evaporation rates under different optical strengths (0.5-2.0 sunlight) were 0.81, 1.30, 1.73, and 1.88 kg m^{-2} h^{-1}, respectively, which indicates that the evaporation rate increases with an increase of solar intensity. To evaluate the solar desalination performance of CMH-HgS_x under actual conditions, a bespoke desalination device was constructed. The simulated sunlight generator was used as the light source and artificial salt water was prepared for the desalination experiments. The evaporated water was collected, and the salt concentration measured using an inductively coupled plasma optical emission spectrometer. From Fig. 5h, the concentration of the four main ions Na(I), Mg(II), Ca(II) and K(I) decreased from 8182.78, 1277.00, 101.53, 289.03 mg L^{-1} to 0.88, 0.22, 0.22; 0.08 mg L^{-1} after the desalination experiment, respectively, which fully complies with the drinking water

542 standards set by the World Health Organization (WHO). The results confirm that CMH-
543 HgS_x has satisfactory purification efficiency. In addition, after eight hours (9:00 am-
544 5:00 pm) under natural sunlight outdoors the solar steam generation measurement
545 experiment (Fig. S13, S14), we observed that the evaporation rate can reach 4.47 kg m^{-2}
546 h^{-1}, and the average solar heat flux was about 79 mW cm^{-2} (in Baoding, the
547 temperature is about 26°C). In addition, the stability is important for determining the
548 real solar steam generation ability of the solar evaporators. As such from Fig. 5i the
549 water evaporation rate of CMH-HgS_x remained unchanged after 5 cycles, implying
550 great photothermal stability in water. These results indicate that the exhausted
551 adsorbents can be upcycled to a photothermal evaporator for practical wastewater
552 treatment.

553 **4. Conclusions**

554 In summary, we report an approach to introduce sulfydryl-based carbon dots (CDs-
555 SH) into a functionalized CMH through hydrogen bonding for the detection and
556 removal of Hg(II) ions from wastewater. CMH-CDs-SH exhibited a rapid response
557 towards Hg(II) over an analytical linear range from 0 to 40 μM. The adsorption
558 experiments confirmed that CMH-CDs-SH exhibits good Hg(II) extraction capacity of
559 over 662.25 mg g^{-1}. In addition, the upcycled material obtained by vulcanization of the
560 saturated adsorbent (CMH-HgS_x) exhibited a high solar steam generation efficiency of
561 about 1.30 kg m^{-2} h^{-1} under one sun irradiation. The upcycled material could be used to
562 adsorb solar irradiation and energy and purify contaminated or sea water, exhibiting

excellent potential for real world applications. Meanwhile, the CMH-HgS_x upcycled material provides a new strategy for the reuse of hazardous waste, thereby reducing environmental pollution. It is expected that our research will provide impetus for the preparation of multifunctional materials suitable for the purification of heavy metal ion in contaminated water and with the ability to be upcycled once saturated for into a material with added value.

Declaration of Competing Interest.

The authors declare that they have no known competing financial interests or personal relationships that could have appeared to influence the work reported in this paper.

Acknowledgements.

The present work is supported by the National Natural Science Foundation of China (Grant #: 21607044). This work was also supported by the Fundamental Research Funds for the Central Universities (Grant #: 2021MS102). TDJ wishes to thank the Royal Society for a Wolfson Research Merit Award and the Open Research Fund of the School of Chemistry and Chemical Engineering, Henan Normal University for support (2020ZD01).

References

[1] N. Abdollahi, S.A.A. Razavi, A. Morsali, M.-L. Hu, High capacity Hg (II) and Pb (II) removal using MOF-based nanocomposite: cooperative effects of pore functionalization and surface-charge modulation, J. Hazard. Mater. 387 (2020) 121667. https://doi.org/https://doi.org/10.1016/j.jhazmat.2019.121667.

[2] X. Liu, R. Ma, X. Wang, Y. Ma, Y. Yang, L. Zhuang, S. Zhang, R. Jehan, J. Chen, X. Wang, Graphene oxide-based materials for efficient removal of heavy metal ions

from aqueous solution: a review, Environ. Pollut. 252 (2019) 62-73. https://doi.org/https://doi.org/10.1016/j.envpol.2019.05.050.
[3] F. Wang, Y. Pan, P. Cai, T. Guo, H. Xiao, Single and binary adsorption of heavy metal ions from aqueous solutions using sugarcane cellulose-based adsorbent, Bioresour. Technol. 241 (2017) 482-490. https://doi.org/https://doi.org/10.1016/j.biortech.2017.05.162.
[4] Z. Qing, L. Zhu, X. Li, S. Yang, Z. Zou, J. Guo, Z. Cao, R. Yang, A target-lighted dsDNA-indicator for high-performance monitoring of mercury pollution and its antagonists screening, Environ. Sci. Technol. 51(20) (2017) 11884-11890. https://doi.org/10.1021/acs.est.7b02858.
[5] D. Zhang, Y. Yao, J. Wu, I. Protsak, W. Lu, X. He, S. Xiao, M. Zhong, T. Chen, J. Yang, Super hydrophilic semi-IPN fluorescent poly(N-(2-hydroxyethyl)acrylamide) hydrogel for ultrafast, selective, and long-term effective mercury(II) detection in a bacteria-laden system, ACS Applied Bio Materials 2(2) (2019) 906-915. https://doi.org/10.1021/acsabm.8b00761.
[6] J.C. Wasserman, L. de Oliveira Silva, G.C. de Pontes, E. de Paiva Lima, Mercury contamination in the sludge of drinking water treatment plants dumping into a reservoir in Rio de Janeiro, Brazil, Environ. Sci. Pollut. R. 25(28) (2018) 28713-28724. https://doi.org/https://doi.org/10.1007/s11356-018-2899-9.
[7] B. Han, Z. Lv, X. Han, S. Li, B. Han, Q. Yang, X. Wang, P. Wu, J. Li, N. Deng, Harmful effects of inorganic mercury exposure on kidney cells: mitochondrial dynamics disorder and excessive oxidative stress, Biol. Trace Elem. Res. (2021) 1-7. https://doi.org/https://doi.org/10.1007/s12011-021-02766-3.
[8] P. Yang, Y. Shu, Q. Zhuang, Y. Li, J. Gu, A robust MOF-based trap with high-density active alkyl thiol for the super-efficient capture of mercury, Chem. Commun. 55(86) (2019) 12972-12975. https://doi.org/https://doi.org/10.1039/C9CC06255F.
[9] C. Xia, S. Zhu, T. Feng, M. Yang, B. Yang, Evolution and synthesis of carbon dots: from carbon dots to carbonized polymer dots, Adv. Sci. 6(23) (2019) 1901316. https://doi.org/ https://doi.org/10.1002/advs.201901316.
[10] Z. Kang, S.-T. Lee, Carbon dots: advances in nanocarbon applications, Nanoscale 11(41) (2019) 19214-19224. https://doi.org/https://doi.org/10.1039/C9NR05647E.
[11] C. Hu, M. Li, J. Qiu, Y.-P. Sun, Design and fabrication of carbon dots for energy conversion and storage, Chem. Soc. Rev. 48(8) (2019) 2315-2337. https://doi.org/https://doi.org/10.1039/C8CS00750K.
[12] M.L. Liu, B.B. Chen, C.M. Li, C.Z. Huang, Carbon dots: synthesis, formation mechanism, fluorescence origin and sensing applications, Green Chem. 21(3) (2019) 449-471. https://doi.org/https://doi.org/10.1039/C8GC02736F.
[13] E. Niyongabo, Y.-C. Jang, D. Kang, K. Sung, Generation, management practices and rapid risk assessment of solid medical wastes: a case study in Burundi, J Mater. Cycles. Waste. 21(4) (2019) 950-961. https://doi.org/https://doi.org/10.1007/s10163-019-00854-0.
[14] F.C. Brown, Y. Bi, S.S. Chopra, K.D. Hristovski, P. Westerhoff, T.L. Theis, End-

of-life heavy metal releases from photovoltaic panels and quantum dot films: hazardous waste concerns or not?, ACS Sustain. Chem. Eng. 6(7) (2018) 9369-9374. https://doi.org/https://doi.org/10.1021/acssuschemeng.8b01705.
[15] Y. Pang, J. Zhang, R. Ma, Z. Qu, E. Lee, T. Luo, Solar–thermal water evaporation: a review, ACS Energy Lett. 5(2) (2020) 437-456. https://doi.org/https://doi.org/10.1021/acsenergylett.9b02611.
[16] R. Li, Y. Shi, M. Alsaedi, M. Wu, L. Shi, P. Wang, Hybrid hydrogel with high water vapor harvesting capacity for deployable solar-driven atmospheric water generator, Environ. Sci. Technol. 52(19) (2018) 11367-11377. https://doi.org/10.1021/acs.est.8b02852.
[17] Y. Shi, C. Zhang, R. Li, S. Zhuo, Y. Jin, L. Shi, S. Hong, J. Chang, C. Ong, P. Wang, Solar evaporator with controlled salt precipitation for zero liquid discharge desalination, Environ. Sci. Technol. 52(20) (2018) 11822-11830. https://doi.org/10.1021/acs.est.8b03300.
[18] H. Ren, M. Tang, B. Guan, K. Wang, J. Yang, F. Wang, M. Wang, J. Shan, Z. Chen, D. Wei, Hierarchical graphene foam for efficient omnidirectional solar–thermal energy conversion, Adv. Mater. 29(38) (2017) 1702590. https://doi.org/https://doi.org/10.1002/adma.201702590.
[19] J. Gong, C. Li, M.R. Wasielewski, Advances in solar energy conversion, Chem. Soc. Rev. 48(7) (2019) 1862-1864. https://doi.org/10.1039/C9CS90020A
[20] M.K.H. Rabaia, M.A. Abdelkareem, E.T. Sayed, K. Elsaid, K.-J. Chae, T. Wilberforce, A. Olabi, Environmental impacts of solar energy systems: a review, Sci. Total Environ. 754 (2021) 141989. https://doi.org/https://doi.org/10.1016/j.scitotenv.2020.141989.
[21] W. Wang, J. Niu, J. Guo, L. Yin, H. Huang, In situ synthesis of PPy-FexOy-CTS nanostructured gel membrane for highly efficient solar steam generation, Sol. Energy Mater. Sol. Cells 201 (2019) 110046. https://doi.org/https://doi.org/10.1016/j.solmat.2019.110046.
[22] S.W. Sharshir, A.M. Algazzar, K. Elmaadawy, A. Kandeal, M. Elkadeem, T. Arunkumar, J. Zang, N. Yang, New hydrogel materials for improving solar water evaporation, desalination and wastewater treatment: a review, Desalination 491 (2020) 114564. https://doi.org/https://doi.org/10.1016/j.desal.2020.114564.
[23] O.P. Ajsuvakova, A.A. Tinkov, M. Aschner, J.B. Rocha, B. Michalke, M.G. Skalnaya, A.V. Skalny, M. Butnariu, M. Dadar, I. Sarac, Sulfhydryl groups as targets of mercury toxicity, Coord. Chem. Rev. 417 (2020) 213343. https://doi.org/https://doi.org/10.1016/j.ccr.2020.213343.
[24] Z. Ma, F. Liu, N. Liu, W. Liu, M. Tong, Facile synthesis of sulfhydryl modified covalent organic frameworks for high efficient Hg (II) removal from water, J. Hazard. Mater. 405 (2021) 124190. https://doi.org/https://doi.org/10.1016/j.jhazmat.2020.124190.
[25] X. Guo, D. Xu, H. Yuan, Q. Luo, S. Tang, L. Liu, Y. Wu, A novel fluorescent nanocellulosic hydrogel based on carbon dots for efficient adsorption and sensitive

671 sensing in heavy metals, J Mater. Chem. A 7(47) (2019) 27081-27088.
672 https://doi.org/https://doi.org/10.1039/C9TA11502A.
673 [26] D. Hu, H. huang, R. Jiang, N. Wang, H. Xu, Y.-G. Wang, X.-k. Ouyang, Adsorption
674 of diclofenac sodium on bilayer amino-functionalized cellulose nanocrystals/chitosan
675 composite, J. Hazard. Mater. 369 (2019) 483-493.
676 https://doi.org/https://doi.org/10.1016/j.jhazmat.2019.02.057.
677 [27] A. Dhillon, D. Kumar, Development of a nanoporous adsorbent for the removal of
678 health-hazardous fluoride ions from aqueous systems, J Mater. Chem. A 3(8) (2015)
679 4215-4228. https://doi.org/https://doi.org/10.1039/C4TA06147K.
680 [28] O. Hakami, Y. Zhang, C.J. Banks, Thiol-functionalised mesoporous silica-coated
681 magnetite nanoparticles for high efficiency removal and recovery of Hg from water,
682 Water Res. 46(12) (2012) 3913-3922.
683 https://doi.org/https://doi.org/10.1016/j.watres.2012.04.032.
684 [29] B. Agarwal, C. Balomajumder, P.K. Thakur, Simultaneous co-adsorptive removal
685 of phenol and cyanide from binary solution using granular activated carbon, Chem. Eng.
686 J 228 (2013) 655-664. https://doi.org/https://doi.org/10.1016/j.cej.2013.05.030.
687 [30] M. Hossain, H. Ngo, W. Guo, L. Nghiem, F. Hai, S. Vigneswaran, T. Nguyen,
688 Competitive adsorption of metals on cabbage waste from multi-metal solutions,
689 Bioresour. Technol. 160 (2014) 79-88.
690 https://doi.org/https://doi.org/10.1016/j.biortech.2013.12.107.
691 [31] R. Laus, V.T. De Favere, Competitive adsorption of Cu (II) and Cd (II) ions by
692 chitosan crosslinked with epichlorohydrin–triphosphate, Bioresour. Technol. 102(19)
693 (2011) 8769-8776. https://doi.org/https://doi.org/10.1016/j.biortech.2011.07.057.
694 [32] C. Mahamadi, T. Nharingo, Competitive adsorption of Pb^{2+}, Cd^{2+} and Zn^{2+} ions
695 onto Eichhornia crassipes in binary and ternary systems, Bioresour. Technol. 101(3)
696 (2010) 859-864. https://doi.org/https://doi.org/10.1016/j.biortech.2009.08.097.
697 [33] F. Zhao, X. Zhou, Y. Shi, X. Qian, M. Alexander, X. Zhao, S. Mendez, R. Yang, L.
698 Qu, G. Yu, Highly efficient solar vapour generation via hierarchically nanostructured
699 gels, Nat. Nanotechnol. 13(6) (2018) 489-495.
700 https://doi.org/https://doi.org/10.1038/s41565-018-0097-z.
701 [34] Y. Han, L. Shi, X. Luo, X. Chen, W. Yang, W. Tang, J. Wang, T. Yue, Z. Li, A
702 signal-on fluorescent sensor for ultra-trace detection of Hg^{2+} via Ag^{+} mediated
703 sulfhydryl functionalized carbon dots, Carbon 149 (2019) 355-363.
704 https://doi.org/https://doi.org/10.1016/j.carbon.2019.04.052.
705 [35] Y. Dong, H. Pang, H.B. Yang, C. Guo, J. Shao, Y. Chi, C.M. Li, T. Yu, Carbon-
706 based dots co-doped with nitrogen and sulfur for high quantum yield and excitation-
707 independent emission, Angew. Chem. Int. Edit. 52(30) (2013) 7800-7804.
708 https://doi.org/https://doi.org/10.1002/anie.201301114.
709 [36] Y.-W. Zeng, D.-K. Ma, W. Wang, J.-J. Chen, L. Zhou, Y.-Z. Zheng, K. Yu, S.-M.
710 Huang, N, S co-doped carbon dots with orange luminescence synthesized through
711 polymerization and carbonization reaction of amino acids, Appl. Surf. Sci. 342 (2015)
712 136-143. https://doi.org/https://doi.org/10.1016/j.apsusc.2015.03.029.

[37] G. Xu, Y. Niu, X. Yang, Z. Jin, Y. Wang, Y. Xu, H. Niu, Preparation of $Ti_3C_2T_x$ MXene-derived quantum dots with white/blue-emitting photoluminescence and electrochemiluminescence, Adv. Opt. Mater. 6(24) (2018) 1800951. https://doi.org/https://doi.org/10.1002/adom.201800951.
[38] J. Liu, Q. Yu, A.R. Showalter, B.A. Bunker, J.S. Swanson, D. Reed, X. Rong, J.B. Fein, Cadmium and proton adsorption onto a halophilic archaeal species: the role of cell envelope sulfhydryl sites, Geochim. Cosmochim. Acta 276 (2020) 186-197. https://doi.org/https://doi.org/10.1016/j.gca.2020.02.038.
[39] M. Zhao, Z. Huang, S. Wang, L. Zhang, Y. Zhou, Design of L-cysteine functionalized UiO-66 MOFs for selective adsorption of Hg (II) in aqueous medium, ACS Appl. Mater. Inter. 11(50) (2019) 46973-46983. https://doi.org/https://doi.org/10.1021/acsami.9b17508.
[40] M.R. Awual, M.M. Hasan, A. Shahat, Functionalized novel mesoporous adsorbent for selective lead (II) ions monitoring and removal from wastewater, Sensor. Actuat. B Chem 203 (2014) 854-863. https://doi.org/https://doi.org/10.1016/j.snb.2014.07.063.
[41] P. Zhao, Y. Yin, W. Cheng, X. Xu, D. Yang, W. Yuan, Development of facile synthesized mesoporous carbon composite adsorbent for efficient CO_2 capture, J CO2 Util. (2021) 101612. https://doi.org/https://doi.org/10.1016/j.jcou.2021.101612.
[42] Y. Ma, Z. Zhang, Y. Xu, M. Ma, B. Chen, L. Wei, L. Xiao, A bright carbon-dot-based fluorescent probe for selective and sensitive detection of mercury ions, Talanta 161 (2016) 476-481. https://doi.org/https://doi.org/10.1016/j.talanta.2016.08.082.
[43] P. Liao, S. Zang, T. Wu, H. Jin, W. Wang, J. Huang, B.Z. Tang, Y. Yan, Generating circularly polarized luminescence from clusterization-triggered emission using solid phase molecular self-assembly, Nat. Commun. 12(1) (2021) 1-9. https://doi.org/https://doi.org/10.1038/s41467-021-25789-9.
[44] Z. Yang, H. Liu, J. Li, K. Yang, Z. Zhang, F. Chen, B. Wang, High-throughput metal trap: sulfhydryl-functionalized wood membrane stacks for rapid and highly efficient heavy metal ion removal, ACS Appl. Mater. Inter. 12(13) (2020) 15002-15011. https://doi.org/https://doi.org/10.1021/acsami.9b19734.
[45] M. Li, X. Li, M. Xu, B. Liu, M. Yang, Z. Chen, T. Gao, T.D. James, L. Wang, H. Xiao, A ratiometric fluorescent hydrogel of controlled thickness prepared continuously using microtomy for the detection and removal of Hg (II), Chem. Eng. J 426 (2021) 131296. https://doi.org/https://doi.org/10.1016/j.cej.2021.131296.
[46] C.-C. Fu, C.-T. Hsieh, R.-S. Juang, J.-W. Yang, S. Gu, Y.A. Gandomi, Highly efficient carbon quantum dot suspensions and membranes for sensitive/selective detection and adsorption/recovery of mercury ions from aqueous solutions, J Taiwan Inst. Chem. E 100 (2019) 127-136. https://doi.org/https://doi.org/10.1016/j.jtice.2019.04.012.
[47] Q. Luo, H. Yuan, M. Zhang, P. Jiang, M. Liu, D. Xu, X. Guo, Y. Wu, A 3D porous fluorescent hydrogel based on amino-modified carbon dots with excellent sorption and sensing abilities for environmentally hazardous Cr (VI), J. Hazard. Mater. 401 (2021) 123432. https://doi.org/https://doi.org/10.1016/j.jhazmat.2020.123432.

[48] F. Almomani, R. Bhosale, M. Khraisheh, T. Almomani, Heavy metal ions removal from industrial wastewater using magnetic nanoparticles (MNP), Appl. Surf. Sci. 506 (2020) 144924. https://doi.org/https://doi.org/10.1016/j.apsusc.2019.144924.
[49] Q. Meng, H. Chen, J. Lin, Z. Lin, J. Sun, Zeolite A synthesized from alkaline assisted pre-activated halloysite for efficient heavy metal removal in polluted river water and industrial wastewater, J Environ. Sci. 56 (2017) 254-262. https://doi.org/https://doi.org/10.1016/j.jes.2016.10.010.
[50] M. Mao, T. Yan, J. Shen, J. Zhang, D. Zhang, Selective capacitive removal of heavy metal ions from wastewater over lewis base sites of S-doped Fe–N–C cathodes via an electro-adsorption process, Environ. Sci. Technol. 55(11) (2021) 7665-7673. https://doi.org/10.1021/acs.est.1c01483.
[51] X. Sun, L. Ji, W. Huang, Z. Li, Y. Liao, K. Xiao, X. Zhu, H. Xu, J. Feng, S. Feng, Z. Qu, N. Yan, Production of H_2S with a novel short-process for the removal of heavy metals in acidic effluents from smelting flue-gas scrubbing systems, Environ. Sci. Technol. 55(6) (2021) 3988-3995. https://doi.org/10.1021/acs.est.0c07884.
[52] Z. Nie, N. Finck, F. Heberling, T. Pruessmann, C. Liu, J. Lützenkirchen, Adsorption of selenium and strontium on goethite: EXAFS study and surface complexation modeling of the ternary systems, Environ. Sci. Technol. 51(7) (2017) 3751-3758. https://doi.org/10.1021/acs.est.6b06104.
[53] X. Wang, Z. Li, Y. Wu, H. Guo, X. Zhang, Y. Yang, H. Mu, J. Duan, Construction of a three-dimensional interpenetrating network sponge for high-efficiency and cavity-enhanced solar-driven wastewater treatment, ACS Appl. Mater. Inter. 13(9) (2021) 10902-10915. https://doi.org/https://doi.org/10.1021/acsami.0c21690.
[54] S.Y. Yoon, S.B. Jang, K.T. Wong, H. Kim, M.J. Kim, C.E. Choong, J.-K. Yang, Y.-Y. Chang, S.-E. Oh, Y. Yoon, Sulfur-anchored palm shell waste-based activated carbon for ultrahigh sorption of Hg (II) for in-situ groundwater treatment, J. Hazard. Mater. 417 (2021) 125995. https://doi.org/https://doi.org/10.1016/j.jhazmat.2021.125995.
[55] C. Jeon, K.L. Solis, H.-R. An, Y. Hong, A.D. Igalavithana, Y.S. Ok, Sustainable removal of Hg (II) by sulfur-modified pine-needle biochar, J. Hazard. Mater. 388 (2020) 122048. https://doi.org/https://doi.org/10.1016/j.jhazmat.2020.122048.
[56] G. Liu, J. Xu, K. Wang, Solar water evaporation by black photothermal sheets, Nano Energy 41 (2017) 269-284. https://doi.org/https://doi.org/10.1016/j.nanoen.2017.09.005.